

## Article

# Structural Phase Transitions in the Double Salts $(\text{NH}_4)_2\text{PO}_3\text{F}\cdot\text{NH}_4\text{NO}_3$ and $(\text{NH}_4)_2\text{XO}_4\cdot 3\text{NH}_4\text{NO}_3$ ( $X = \text{Se}, \text{Cr}$ )

Matthias Weil <sup>1,\*</sup> , Thomas Häusler <sup>1</sup>, Barbara Bonneau <sup>2</sup> and Ekkehard Füglein <sup>3</sup>

<sup>1</sup> Institute for Chemical Technologies and Analytics, Division of Structural Chemistry, TU Wien, Getreidemarkt 9/E164-05-1, Vienna 1060, Austria

<sup>2</sup> IUT Bordeaux, 15 Rue Naudet, 33175 Gradignan, France

<sup>3</sup> Netzsch-Gerätebau GmbH, Wittelsbacherstr. 42, 95100 Selb, Germany; ekkehard.fueglein@netzsch.com

\* Correspondence: matthias.weil@tuwien.ac.at

**Abstract:** In the context of investigating isostructural relationships between sulfates and monofluorophosphates, crystals of the double salts  $(\text{NH}_4)_2\text{PO}_3\text{F}\cdot\text{NH}_4\text{NO}_3$  (AFP·AN) and  $(\text{NH}_4)_2\text{XO}_4\cdot 3\text{NH}_4\text{NO}_3$  (AX·3AN;  $X = \text{Se}, \text{Cr}$ ) were grown from aqueous solutions and structurally characterized using X-ray diffraction and thermal analysis. Whereas the high-temperature forms of the two AX·3AN double salts are in fact isostructural with the sulfate analogue, AFP·AN crystallizes with a reduced amount of  $\text{NH}_4\text{NO}_3$  and thus has a unique crystal structure. Both AFP·AN and the two AX·3AN compounds exhibit reversible structural phase transitions. Upon cooling, the monofluorophosphate double salt transforms from the monoclinic room-temperature polymorph (I;  $P2_1/n$ ,  $Z = 4$ ) to the intermediate triclinic polymorph (II;  $P1$ ,  $Z = 4$ ) that in turn transforms to the monoclinic low-temperature polymorph (III;  $P2_1/n$ ,  $Z = 4$ ). The two phase transitions (I)  $\rightarrow$  (II) and (II)  $\rightarrow$  (III) are characterized by a significant increase of the unit cell volumes upon cooling. The two AX·3AN double salts transform upon cooling from a disordered monoclinic crystal structure ( $P2_1$ ,  $Z = 2$ ) to a monoclinic polymorph with a doubled unit cell ( $P2_1/c$ ,  $Z = 4$ ). Such a phase transition is not observed for the sulfate analogue. All molecular moieties are fully ordered at  $-93^\circ\text{C}$  for the selenate double salt, whereas one of the nitrate anions remains disordered for the chromate double salt even at  $-173^\circ\text{C}$ . In all AFP·AN and AX·3AN crystal structures, the nitrate anions play a crucial role during the phase transitions, and an extensive network of N–H $\cdots$ O hydrogen-bonding interactions is responsible for the cohesion of the crystal.

**Keywords:** monofluorophosphate; double salt; crystal structure determination; phase transition; polytypism; isotypism; hydrogen bonding; quantitative structural comparison



**Citation:** Weil, M.; Häusler, T.; Bonneau, B.; Füglein, E. Structural Phase Transitions in the Double Salts  $(\text{NH}_4)_2\text{PO}_3\text{F}\cdot\text{NH}_4\text{NO}_3$  and  $(\text{NH}_4)_2\text{XO}_4\cdot 3\text{NH}_4\text{NO}_3$  ( $X = \text{Se}, \text{Cr}$ ). *Inorganics* **2023**, *11*, 433. <https://doi.org/10.3390/inorganics11110433>

Academic Editors: Richard Dronskowski, Christian Julien, Rainer Niewa, Guido Kickelbick, Alexander S. Novikov, Gary Hix and Hans-Conrad zur Loye

Received: 13 September 2023

Revised: 10 October 2023

Accepted: 16 October 2023

Published: 8 November 2023



**Copyright:** © 2023 by the authors. Licensee MDPI, Basel, Switzerland. This article is an open access article distributed under the terms and conditions of the Creative Commons Attribution (CC BY) license (<https://creativecommons.org/licenses/by/4.0/>).

## 1. Introduction

Monofluorophosphates comprising the  $\text{PO}_3\text{F}^{2-}$  anion have many applications. They are used as wood preservatives, corrosion inhibitors, solubility inhibitors for lead in potable water sources, or as active agents against osteoporosis. The most commonly used monofluorophosphate is  $\text{Na}_2\text{PO}_3\text{F}$ , which is added to some toothpaste as a fluorine source for the protection of tooth enamel to avoid caries [1]. More recently, monofluorophosphates are also used as materials exhibiting nonlinear optical (NLO) behavior [2].

Willy Lange, who discovered the family of monofluorophosphates more than 90 years ago, emphasized the chemical relationships between monofluorophosphates and sulfates in terms of solubilities and reaction behaviors [3]. The tetrahedral  $\text{PO}_3\text{F}^{2-}$  and  $\text{SO}_4^{2-}$  anions are isoster and isoelectronic. In fact, it was reported that some monofluorophosphates and sulfates of the same formula type are *isomorphic*, but without proof of the respective crystal structures [4]. It is noted that the terms *isomorphic/isomorphism* still are found in the (recent) literature to express structural relationships, but their use is not recommended any longer. More appropriate terms are *isostructural/isostructurality* or synonymously *isotypic/isotypism* [5].

In a recent survey on the crystal chemistry of monofluorophosphates, it was shown that—contrary to the original report [4]—they are in most cases not structurally closely related to the corresponding sulfates, and only in a few cases, an isostructural relationship is found [6]. In this context, the current investigation was initiated to check whether a corresponding monofluorophosphate phase exists for the ammonium sulfate (AS)/ammonium nitrate (AN) double salts  $(\text{NH}_4)_2\text{SO}_4 \cdot 2\text{NH}_4\text{NO}_3$  (AS·2AN) and  $(\text{NH}_4)_2\text{SO}_4 \cdot 3\text{NH}_4\text{NO}_3$  (AS·3AN) [7] and, if so, whether there is an isostructural relationship. In addition, phase formation studies were also conducted for the double salt systems  $(\text{NH}_4)_2\text{XO}_4/\text{NH}_4\text{NO}_3$  with related tetrahedral  $\text{XO}_4^{2-}$  anions ( $X = \text{Se}, \text{Cr}$ ).

## 2. Materials and Methods

### 2.1. Crystallization Studies

Commercially available chemicals of practical grade originated from Merck (Darmstadt, Germany). Anhydrous  $(\text{NH}_4)_2\text{PO}_3\text{F}$  (AFP) was prepared from a urea melt according to the protocol reported by Schülke and Kayser [8]. The polycrystalline material was then recrystallized from an acetone/water mixture (2/1 *v/v*), obtaining the monohydrate  $(\text{NH}_4)_2\text{PO}_3\text{F} \cdot \text{H}_2\text{O}$  [9] as phase-pure material. The latter was used as the monofluorophosphate source in subsequent crystal growth experiments.

Phase formation studies in the system AFP/AN were conducted at room temperature with aqueous ammonium monofluorophosphate and ammonium nitrate stock solutions ( $2.5 \cdot 10^{-2}$  mol in 15 mL water in each case). The two solutions were mixed in polypropylene beakers in different molar ratios (3:1, 2:1, 1:1, 1:2, 1:3). The mixtures were then allowed to crystallize within one week at room temperature under full evaporation of water.

$(\text{NH}_4)_2\text{SeO}_4$  (ASe) was prepared via the neutralization of a diluted aqueous solution of selenic acid (80%<sub>wt</sub>), with an aqueous ammonia solution (25%<sub>wt</sub>) and subsequent evaporation of water. The obtained crude product was recrystallized from water.  $(\text{NH}_4)_2\text{CrO}_4$  (ACr) was used without purification. Phase formation studies in the AX/AN ( $X = \text{Se}, \text{Cr}$ ) systems were conducted in the same way as described above. For the ACr/AN system, only crystallization experiments with a molar ratio of 1:3 were performed both at room temperature and at 8 °C in a refrigerator.

In each case, the resulting bulk material was then analyzed using powder X-ray diffraction (PXRD). Crystals suitable for single-crystal X-ray diffraction were sorted from selected batches.

### 2.2. Thermal Analysis

For the low-temperature differential scanning calorimetry (DSC) measurement of AFP·AN, a Netzsch DSC 204 F1 Phoenix instrument (Netzsch Gerätebau, Selb, Germany) was used (temperature ranged from 30 °C to −160 °C in two cycles; sample mass 17.2 mg, nitrogen atmosphere with a flow rate of 20 mL·min<sup>−1</sup>, heating-/cooling rate 10 °C·min<sup>−1</sup>, pierced aluminum crucible with 25 μL inner volume). Thermogravimetry (TG) and all other DSC measurements were carried out under flowing argon atmosphere conditions (20 mL·min<sup>−1</sup>) using a Netzsch TG 209 F3 Tarsus (heating rate 10 °C·min<sup>−1</sup>) and a Netzsch DSC 200 F3 Maia instrument (heating/cooling rate 10 °C·min<sup>−1</sup>, pierced aluminum crucible with 25 μL inner volume, ~15 mg loading), respectively. For the TG measurement (loading ~30 mg), an alumina crucible with an inner volume of 85 μL and with a pierced alumina lid was used as the sample container. A correction measurement of the empty crucible was conducted and afterwards subtracted from the measurement data.

### 2.3. X-ray Diffraction Measurements and Crystal-Structure Analysis

PXRD measurements were performed at room temperature on a PANalytical X'Pert II Pro-type PW 3040/60 diffractometer using Cu-K $\alpha$  radiation and an X'Celerator detector (Malvern Panalytical, Malvern, United Kingdom). For phase analysis and Rietveld refinements of the reaction products, the Highscore+ software suite (version 5.1) [10] was employed. For temperature-dependent measurements upon cooling, the diffractometer

was equipped with a PheniX closed-cycle helium cryostat (Oxford Cryosystems, Long Hanborough, Oxford, United Kingdom). The sample was measured in 7.5 °C steps from room temperature to −220 °C, with a holding time of 10 min for each step. For temperature-dependent measurements upon heating, the diffractometer was equipped with an Anton Paar TTK-450 chamber (Anton Paar GmbH, Graz, Austria) using measurements ranging from 25 °C to 80 °C with steps of 4 °C and a holding time of 5 min for each step before measurement.

Single-crystal X-ray diffraction measurements were performed at different temperatures on a Bruker Kappa APEX-II single-crystal diffractometer (Bruker AXS, Madison, WI, USA) using graphite-monochromatized Mo-K $\alpha$  radiation equipped with a CCD detector and an Oxford Cryosystems cooling/heating device operating at the adjusted temperature with a stream of nitrogen. Instrument software (APEX2, SAINT [11]) was used for optimized diffraction measurement strategies and for data reduction; correction for absorption effects was performed using SADABS [12], and TWINABS [11] for twinned crystals. The crystal structures were solved using SHELXS [13], refined using SHELXL [14], and graphically represented using ATOMS [15].

Twinning by non-merohedry was observed for the low-temperature polymorph AFP·AN-(III), and only the data of the major twin domain and non-overlapping reflections were processed. To account for a similar unit cell setting of the three AFP·AN polymorphs, the unit cell setting of the intermediate triclinic AFP·AN-(II) polymorph was chosen as being non-reduced [16].

For the crystal structures of the high-temperature AX·3AN-(I) polymorphs in space group  $P2_1$ , the same atom labelling, starting atomic coordinates, and rotational disorder model for one of the nitrate groups corresponding to the isotopic sulfate analog AS·3AN [7] were used. Checking for possible higher symmetry was performed using PLATON [17]. A provisional check using the *Addsym* routine suggested space group  $P2_1/m$ , but a detailed check using *Addsym-EXT* and testing the suggested model did not lead to a meaningful result. For the low-temperature AX·3AN-(II) polymorphs in the space group  $P2_1/c$ , atom labels and coordinates were chosen as the most similar to the high-temperature polymorphs. The occurrence of rotational disorder of nitrate groups in the low-temperature polymorphs was treated the same way as in the high-temperature polymorphs. For all AFP·AN and AX·3AN structures, H atoms of ammonium groups were found from difference electron density maps. They were refined using a common  $U_{\text{iso}}$  parameter, with a constrained N–H distance of 0.90(2) Å.

Table 1 lists crystal structure and refinement data for the three AFP·AN polymorphs at −73 °C, −98 °C, and −173 °C, and Table 2 lists the high-temperature polymorphs of AX·3AN and their low-temperature polymorphs at −173 °C. Data resulting from measurements at 22 °C (AFP·AN), −23 °C, −73 °C, and −123 °C (AX·3AN) are collated in the Supplementary Material (Tables S1–S4). Further details of the crystal structure investigations may be obtained from the joint CCDC/FIZ Karlsruhe online deposition service at <https://www.ccdc.cam.ac.uk/structures/> by quoting the deposition numbers specified at the end of each of these tables.

**Table 1.** Data collection and refinement details of  $(\text{NH}_4)_2\text{PO}_3\text{F}\cdot\text{NH}_4\text{NO}_3$  polymorphs.

	$(\text{NH}_4)_2\text{PO}_3\text{F}\cdot\text{NH}_4\text{NO}_3\text{-(I)}$	$(\text{NH}_4)_2\text{PO}_3\text{F}\cdot\text{NH}_4\text{NO}_3\text{-(II)}$	$(\text{NH}_4)_2\text{PO}_3\text{F}\cdot\text{NH}_4\text{NO}_3\text{-(III)}$
Code	AFP·AN-(I)	AFP·AN-(II)	AFP·AN-(III)
$M_r$	214.11	214.11	214.11
Space group, No	$P2_1/n$ , 14	$P1$ , 2	$P2_1/n$ , 14
$Z$	4	4	4
Temperature/°C	−73	−98	−173
Crystal form, color	plate, colourless	plate, colourless	plate, colourless
Crystal dimension/mm <sup>3</sup>	$0.55 \times 0.45 \times 0.10$	$0.45 \times 0.35 \times 0.08$	$0.35 \times 0.30 \times 0.06$
$a/\text{Å}$	10.3145(7)	10.3414(4)	10.3182(9)
$b/\text{Å}$	6.1035(4)	6.1056(2)	6.0591(6)
$c/\text{Å}$	14.3299(10)	14.1704(7)	14.3715(12)
$\alpha/^\circ$	90	91.248(3)	90
$\beta/^\circ$	103.885(2)	101.016(2)	98.563(2)
$\gamma/^\circ$	90	89.173(2)	90
$V/\text{Å}^3$	875.77(10)	877.98(6)	888.48(14)
X-ray density/g·cm <sup>−3</sup>	1.624	1.620	1.601
Radiation type	Mo $K\alpha$	Mo $K\alpha$	Mo $K\alpha$
$\mu/\text{mm}^{-1}$	0.339	0.338	0.334
$T_{\min}$ , $T_{\max}$	0.680, 0.747	0.697, 0.748	0.624, 0.746
No. of measured, independent, and observed [ $I$ > $2\sigma(I)$ ] reflections	45048, 3653, 3111	101011, 11763, 9079	3260, 3260, 2903
$R_{\text{int}}$	0.0569	0.0425	—
$(\sin \theta/\lambda)_{\text{max}}/\text{Å}^{-1}$	0.801	0.932	0.760
No. of reflections	3653	11,763	3260
No. of parameters	147	290	147
$R[F^2 > 2\sigma(F^2)]$ , $wR(F^2)$ , $S$	0.028, 0.074, 1.10	0.031, 0.081, 1.05	0.027, 0.069, 1.08
$\Delta\rho_{\text{max}}$ , $\Delta\rho_{\text{min}}$ ( $\text{e}^- \cdot \text{Å}^{-3}$ )	0.52, −0.34	0.65, −0.52	0.40, −0.28
CSD-code	2294159	2294161	2294148

Crystal structures of the same symmetry and the same number of atoms in the asymmetric unit (AFP·AN-(I) and -(III)) or isotopic crystal structures were quantitatively compared using the *compstru* program [20] available at the Bilbao crystallographic server [21].

#### 2.4. Infrared (IR) Spectroscopy

IR measurements of AFP·AN-(I) were carried out at room temperature in a diamond attenuated total reflection (ATR) accessory using a Bruker Tensor 27 FT-IR spectrometer (Bruker Corporation, Billerica, MA, USA). Samples were ground to fine powder prior to the investigation. The spectra in a range of 4000–400  $\text{cm}^{-1}$  were obtained as an average of four consecutive individual measurements.

**Table 2.** Data collection and refinement details of  $(\text{NH}_4)_2\text{XO}_4 \cdot 3\text{NH}_4\text{NO}_3$  polymorphs ( $X = \text{Se}, \text{Cr}$ ).

	$(\text{NH}_4)_2\text{SeO}_4 \cdot 3\text{NH}_4\text{NO}_3$ - <b>(I)</b>	$(\text{NH}_4)_2\text{SeO}_4 \cdot 3\text{NH}_4\text{NO}_3$ - <b>(II)</b>	$(\text{NH}_4)_2\text{CrO}_4 \cdot 3\text{NH}_4\text{NO}_3$ - <b>(I)</b>	$(\text{NH}_4)_2\text{CrO}_4 \cdot 3\text{NH}_4\text{NO}_3$ - <b>(II)</b>
Code	ASe·3AN-(I)	ASe·3AN-(II)	ACr·3AN-(I)	ACr·3AN-(II)
$M_r$	419.20	419.20	392.24	392.24
Space group, No	$P2_1, 4$	$P2_1/c, 14$	$P2_1, 4$	$P2_1/c, 14$
Z	2	4	2	4
Temperature/ $^\circ\text{C}$	50	−173	60	−173
Crystal form, color	plate, colourless	plate, colourless	plate, yellow	plate, yellow
Crystal dimension/ $\text{mm}^3$	$0.30 \times 0.20 \times 0.05$	$0.30 \times 0.20 \times 0.05$	$0.08 \times 0.08 \times 0.01$	$0.08 \times 0.08 \times 0.01$
$a/\text{Å}$	10.0933(8)	10.0343(8)	10.049(4)	9.9417(13)
$b/\text{Å}$	6.0117(5)	6.0652(5)	5.956(2)	5.9118(8)
$c/\text{Å}$	12.5641(11)	24.331(2)	12.576(5)	24.843(3)
$\alpha/^\circ$	90	90	90	90
$\beta/^\circ$	92.714(2)	93.218(2)	92.474(9)	92.546(3)
$\gamma/^\circ$	90	90	90	90
$V/\text{Å}^3$	761.51(11)	1478.5(2)	751.9(5)	1458.7(3)
X-ray density/ $\text{g}\cdot\text{cm}^{-3}$	1.828	1.883	1.732	1.786
Radiation type	Mo $K\alpha$	Mo $K\alpha$	Mo $K\alpha$	Mo $K\alpha$
$\mu/\text{mm}^{-1}$	2.548	2.625	0.840	0.870
$T_{\min}, T_{\max}$	0.697, 0.748	0.611, 0.747	0.667, 0.787	0.663, 0.747
No. of measured, independent, and observed [ $I > 2\sigma(I)$ ] reflections	48670, 7102, 5846	80103, 6547, 5767	28070, 5541, 3256	44239, 4249, 3428
$R_{\text{int}}$	0.0366	0.0384	0.1090	0.0537
$(\sin \theta/\lambda)_{\text{max}}/\text{Å}^{-1}$	0.824	0.817	0.765	0.703
No. of reflections	7102	6547	5541	4249
No. of parameters	228	260	228	288
$R[F^2 > 2\sigma(F^2)], wR(F^2), S$	0.033, 0.087, 1.07	0.021, 0.049, 1.07	0.059, 0.186, 0.98	0.037, 0.101, 1.03
$\Delta\rho_{\text{max}}, \Delta\rho_{\text{min}} (\text{e}^- \cdot \text{Å}^{-3})$	0.65, −0.52	1.10, −0.54	1.05, −0.56	1.40, −0.61
Absolute structure	Refined as an inversion twin; Flack 0.518(11)	—	Refined as an inversion twin; Flack 0.58(6)	—
CSD-code	2294151	2294157	2294149	2294155

Bond valence calculations [18] were performed using the parameters of Brese and O'Keeffe [19], which are listed in Table 3 for AFP·AN and in Table 4 for AX·3AN.

**Table 3.** Selected bond lengths, interactions/Å, bond angles/° and bond valence sums (BVS)/valence units of AFP·AN polymorphs.

AFP·AN-(I) at −73 °C			
P1—O2	1.4982(6)	N1—O6	1.2444(11)
P1—O3	1.5080(6)	N1—O5	1.2463(13)
P1—O1	1.5106(6)	N1—O4	1.2464(11)
P1—F1	1.5953(6)		
O2—P1—O3	115.38(4)	O2—P1—F1	104.20(4)
O2—P1—O1	115.01(4)	O3—P1—F1	103.51(4)
O3—P1—O1	113.82(4)	O1—P1—F1	102.72(3)
N...O	2.7624(11)–3.0200(14)		
BVS: P1 4.92, N1: 4.96			
AFP·AN-(II) at −98 °C			
P1A—O3A	1.4995(5)	N1A—O4A	1.2360(9)
P1A—O2A	1.5098(5)	N1A—O5A	1.2529(9)
P1A—O1A	1.5157(5)	N1A—O6A	1.2613(9)
P1A—F1A	1.5928(5)	N1B—O6B	1.2462(10)
P1B—O2B	1.5046(5)	N1B—O5B <sup>iii</sup>	1.2492(9)
P1B—O3B	1.5058(5)	N1B—O4B	1.2519(9)
P1B—O1B	1.5125(5)		
P1B—F1B	1.6021(4)		
O3A—P1A—O2A	115.03(3)	O2B—P1B—O3B	115.41(3)
O3A—P1A—O1A	115.41(3)	O2B—P1B—O1B	115.59(3)
O2A—P1A—O1A	113.33(3)	O3B—P1B—O1B	114.16(3)
O3A—P1A—F1A	104.86(3)	O2B—P1B—F1B	103.17(3)
O2A—P1A—F1A	103.77(3)	O3B—P1B—F1B	103.35(3)
O1A—P1A—F1A	102.37(3)	O1B—P1B—F1B	102.65(3)
N...O	2.7890(8)–3.0515(11)		
BVS: P1A 4.89, P1B 4.88 N1A: 4.90, N1B 4.92			
AFP·AN-(III) at −173 °C			
P1—O2	1.5059(6)	N1—O4	1.2357(10)
P1—O3	1.5100(6)	N1—O5	1.2565(10)
P1—O1	1.5164(6)	N1—O6	1.2696(10)
P1—F1	1.5992(5)		
O2—P1—O3	115.13(3)	O2—P1—F1	103.56(3)
O2—P1—O1	115.72(4)	O3—P1—F1	103.80(3)
O3—P1—O1	113.73(3)	O1—P1—F1	102.58(3)
N...O	2.7811(10)–2.9446(9)		
BVS: P1 4.85, N1: 4.86			

**Table 4.** Selected bond lengths, interactions/ $\text{\AA}$ , and bond valence sum (BVS)/valence units of AX·3AN polymorphs (X = Se, Cr).

ASe·3AN-(I) at 50 °C			
Se1—O1	1.608(4)	N2—O8	1.233(5)
Se1—O4	1.611(3)	N2—O10	1.253(3)
Se1—O3	1.626(3)	N2—O9	1.264(5)
Se1—O2	1.627(2)	N3—O13B	1.15(2)
N1—O6	1.190(8)	N3—O11B	1.150(18)
N1—O5	1.195(4)	N3—O12A	1.171(6)
N1—O7	1.279(8)	N3—O13A	1.253(6)
N...O	2.721(4)–3.159(5)	N3—O11A	1.262(5)
BVS: Se1 6.34, N1 5.33, N2 4.91, N3 5.07		N3—O12B	1.365(14)
ASe·3AN-(II) at –173 °C			
Se1—O3	1.6351(7)	N2—O8	1.2550(11)
Se1—O4	1.6370(7)	N2—O9	1.2569(11)
Se1—O1	1.6406(7)	N2—O10	1.2594(11)
Se1—O2	1.6522(7)	N3—O12	1.2348(12)
N1—O5	1.2444(11)	N3—O11	1.2412(11)
N1—O6	1.2501(11)	N3—O13	1.2702(11)
N1—O7	1.2654(10)		1.253
N...O	2.7654(11)–3.1260(12)		
BVS: Se1 5.95, N1 4.8, N2 4.82, N3 4.93			
ACr·3AN-(I) at 60 °C			
Cr1—O1	1.589(6)	N2—O9	1.206(10)
Cr1—O4	1.622(4)	N2—O10	1.253(5)
Cr1—O2	1.657(3)	N2—O8	1.315(10)
Cr1—O3	1.694(6)	N3—O11B	1.10(2)
N1—O5	1.192(7)	N3—O12A	1.135(8)
N1—O7	1.197(11)	N3—O11A	1.280(9)
N1—O6	1.281(13)	N3—O12B	1.313(19)
N...O	2.735(6)–3.164(14)	N3—O13B	1.34(3)
BVS: Cr1 6.09, N1 5.30, N2 4.84, N3 5.11.		N3—O13A	1.343(14)
ACr·3AN-(II) at –173 °C			
Cr1—O3	1.6380(13)	N2—O10	1.255(2)
Cr1—O4	1.6394(15)	N2—O9	1.2549(19)
Cr1—O1	1.6473(14)	N2—O8	1.259(2)
Cr1—O2	1.6656(13)	N3—O12	1.219(2)
N1—O5A	1.103(7)	N3—O11	1.249(2)
N1—O6B	1.110(6)	N3—O13	1.264(2)
N1—O7A	1.294(4)	N...O	2.741(2)–3.154(3)
N1—O7B	1.304(4)		
N1—O5B	1.353(6)		
N1—O6A	1.379(6)		
BVS: Cr 5.95, N1 5.31, N2 4.82, N3 4.99			

### 3. Results and Discussion

#### 3.1. Crystallization

The phase analysis of PXRD data revealed that in the AFP/AN system, only the batch with a molar ratio of AFP:AN = 1:1 resulted in the formation of a new AFP·AN compound in the form of a single-phase product. All other batches resulted in the crystallization of one of the educts and AFP·AN in varying amounts. A similar result was obtained in the ASe/AN system. However, only the batch with a molar ratio of ASe:AN = 1:3 resulted in a single-phase product of ASe·3AN, and all other batches showed the presence of one of the educts and of the selenate double salt. Due to the hazardous nature of the educt ACr, we performed only a minimum amount of crystallization experiments in the system ACr/AN. Based on the successful crystallization in the related ASe/AN system, we chose a molar ratio of ACr:AN = 1:3. The corresponding product ACr·3AN that crystallized at room

temperature did not contain crystals suitable for single-crystal X-ray diffraction. Repeated crystallization at 8 °C resulted in useful crystals in this respect, but they were of poorer quality in direct comparison with the crystals of the selenate double salt.

### 3.2. Thermal Behavior

#### 3.2.1. AFP·AN

AFP·AN exhibits two reversible phase transitions upon cooling and reheating as revealed by DSC measurements (Figure 1). Under these conditions, the room temperature form AFP·AN-(I) transforms exothermally at  $-97.5$  °C (onset) into the intermediate phase AFP·AN-(II), which in turn transforms exothermally into AFP·AN-(III) at  $-106.5$  °C (onset). Upon reheating, the stepwise endothermic retransition takes place with a hysteresis of about 7 °C, i.e., the transition from polymorph-(III)  $\rightarrow$  polymorph-(II)  $\rightarrow$  polymorph-(I) at  $-102.8$  °C and  $-88.6$  °C, respectively. The almost congruent course of the cycled cooling and heating curves indicates the reproducibility of the reversible reactions.

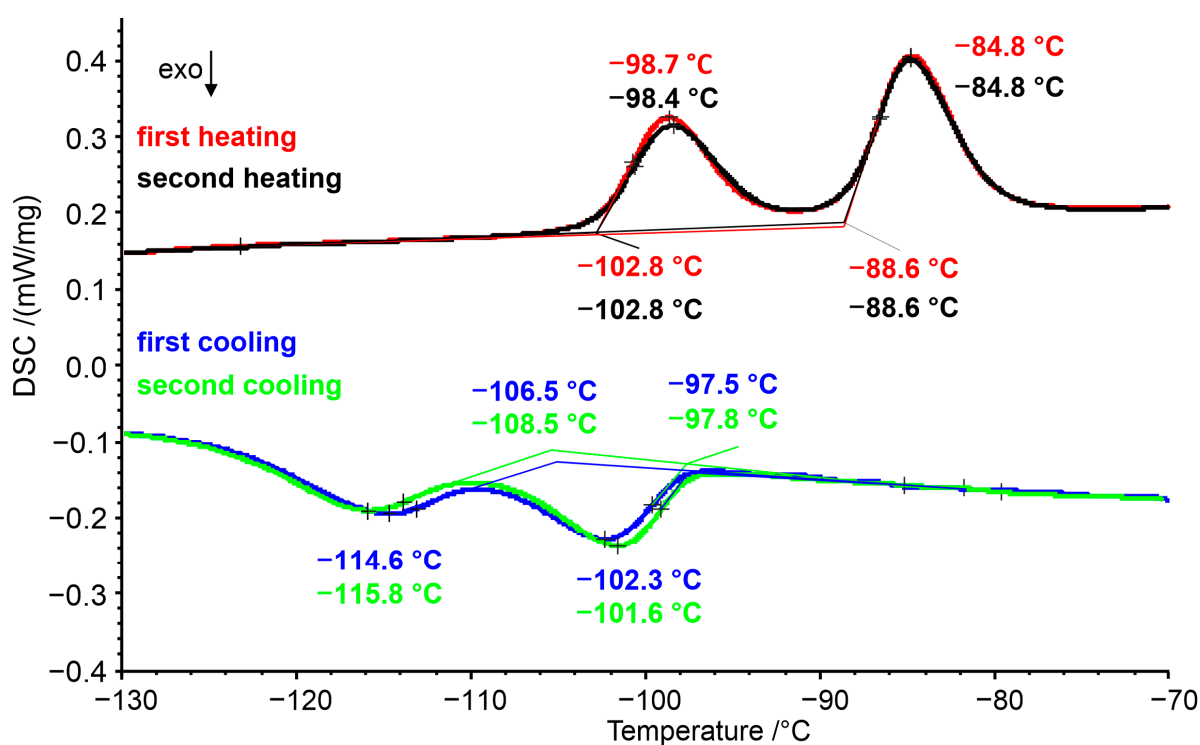


**Figure 1.** Two-cycle DSC measurement of AFP·AN indicating the reversibility and reproducibility of the two phase transitions. The onset and peak maxima temperatures are shown. The initial temperature range for measurement (30 °C to  $-160$  °C) was minimized for better visibility of the phase transitions.

For single crystal X-ray diffraction measurements, the phase transition from polymorph-(I)  $\rightarrow$  polymorph-(II) was monitored by stepwise cooling from  $-73$  °C until a significant change in the diffraction pattern was observed. Under these conditions, the phase transition was complete at  $-98$ °.

In order to confirm the phase transitions and crystal structures of the AFP·AN polymorphs, temperature-dependent PXRD measurements were performed under cooling. As shown in Figure 2, the two phase transitions are clearly visible by a change in the diffraction pattern. Under these conditions, the first transition takes place at  $\sim -106$  °C, and the second at  $\sim -130$  °C. The transition temperatures determined by DSC and temperature-dependent PXRD differ ( $-97.5$  °C,  $-106.5$  °C versus  $-106$  °C,  $-130$  °C), which is caused by different heating rates, holding and measurement times and, most importantly, by different place-

ments of the thermocouple relative to the sample. Polymorph-(III) is stable upon cooling until at least  $-220\text{ }^{\circ}\text{C}$  according to temperature-dependent PXRD.

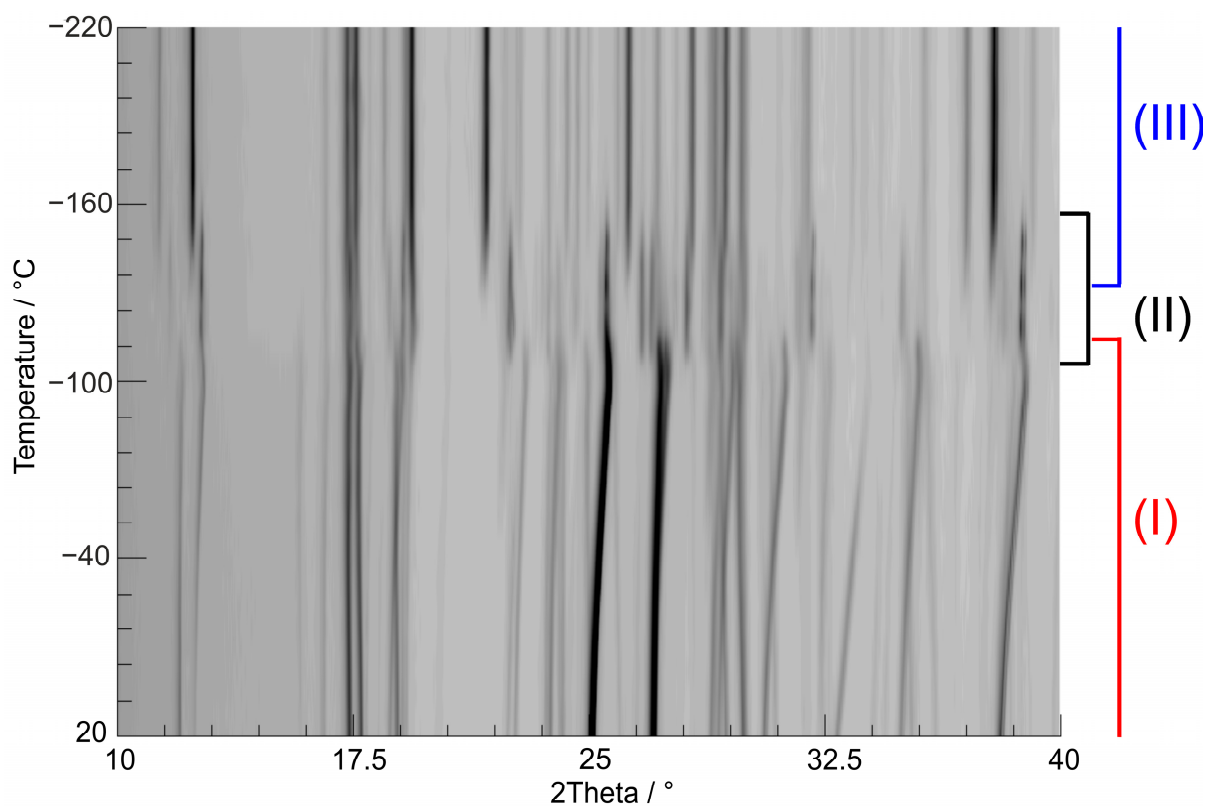


**Figure 2.** Temperature-dependent PXRD measurement of AFP·AN. The stability fields of polymorphs-(I), -(II) and -(III) are indicated on the right-hand side.

Experimental PXRD data and corresponding simulations (Supplementary Material, Figure S1) are in good agreement, which allowed us to evaluate the temperature-dependent evolution of unit cell parameters on the basis of Rietveld refinements. While for each polymorph a decrease in temperature leads to the expected decrease in the volume of the unit cell, there is a considerable jump in volume during the two phase transitions (Figure 3). Hence, the densities stepwise decrease from polymorph-(I)  $\rightarrow$  polymorph-(II)  $\rightarrow$  polymorph-(III) (see also Table 1), although the exothermic formation of the latter shows it to be the thermodynamically stable phase. In this regard, AFP·AN does not follow the Ostwald–Volmer rule, according to which the metastable and less dense phases form first under energy reduction.

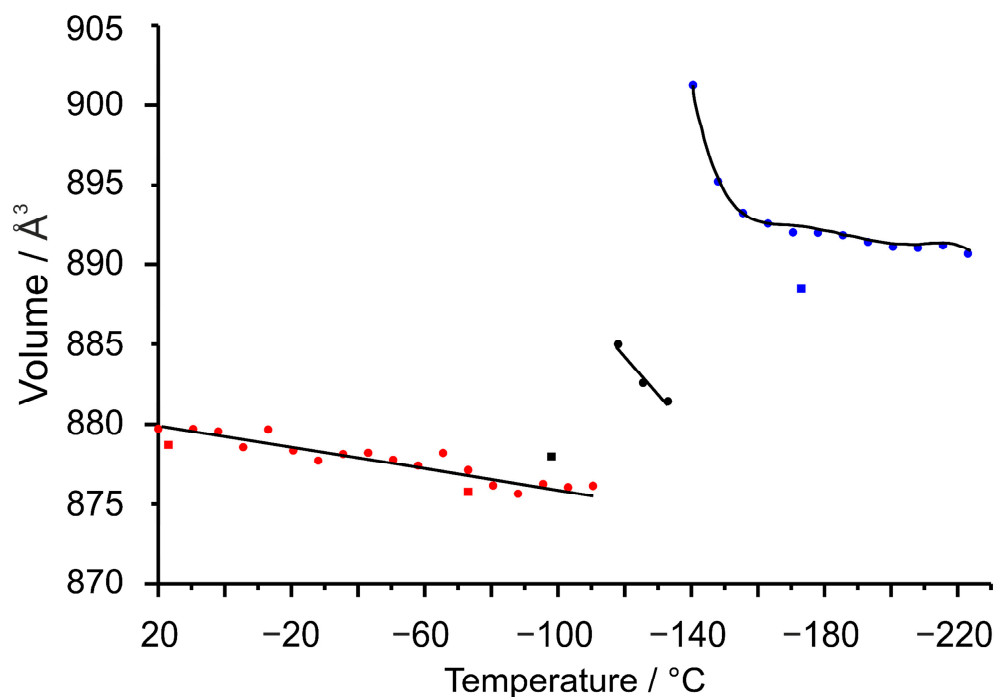
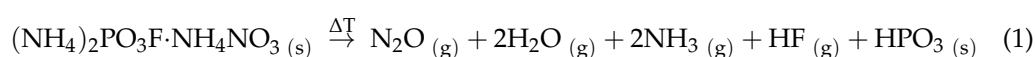


**Figure 3.** Evolution of the unit cell volume of AFP·AN polymorphs-(I) (red), -(II) (black), and -(III) (blue) upon cooling, as determined by Rietveld refinements (dots; the regression curves serve as a guide for the eye). Single-crystal data are indicated by squares in the corresponding color.

Upon heating, AFP·AN is stable until ~180 °C when it starts to decompose in multiple steps to yield a product at 300 °C, which gradually decomposes further (Supplementary Material, Figure S2). The finally obtained product at 550 °C is X-ray amorphous and most likely corresponds to metaphosphoric acid, HPO<sub>3</sub>, a compound that can be prepared using the thermal decomposition of (NH<sub>4</sub>)<sub>2</sub>HPO<sub>4</sub> at 500 °C [22]. The idealized overall thermal decomposition of AFP·AN can thus be formulated according to Equation (1) (mass loss: theory 62.6%; exp. at 500 °C 66.5%):



### 3.2.2. AX·3AN

DSC measurements of ASe·3AN and ACr·3AN revealed a reversible phase transition slightly above room temperature in each case (Figure 4). Upon heating, both compounds transform endothermally from the room-temperature polymorph-(II) to the high-temperature polymorph-(I). The determined transition temperature of 38.7 °C (onset) for the selenate double salt is in good agreement with that from temperature-dependent PXRD data, for which Rietveld refinements showed a jump of the unit cell volume between 37 °C and 40 °C (Supplementary Material, Figure S3). Upon cooling in the DSC instrument, retransition occurs with a slight hysteresis for the selenate at 36.6 °C. For the chromate double salt, the phase transition onset temperatures were determined at 52 °C upon heating and 45.2 °C upon cooling using the DSC measurement (temperature-dependent PXRD not performed). For the chromate double salt, there is also a very small reversible effect at about −10 °C that could not be assigned to another structural phase transition on the basis of the current single-crystal X-ray data.

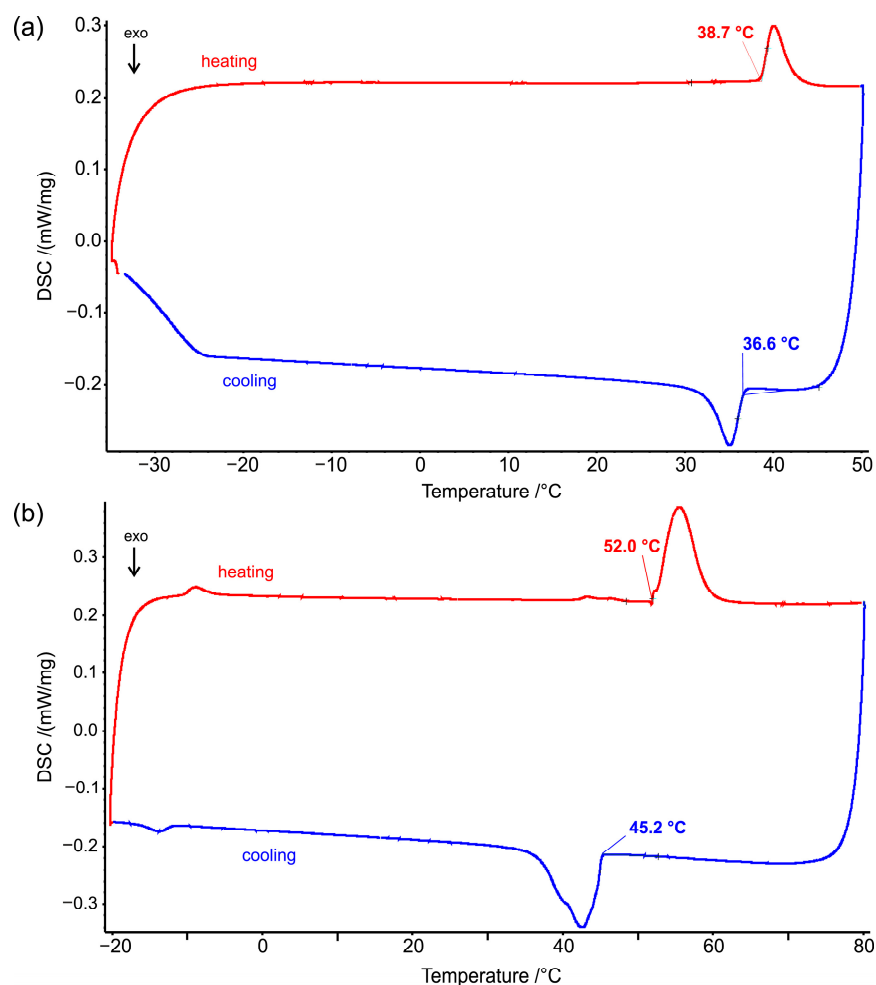


**Figure 4.** DSC measurements of ASe·3AN (a) and ACr·3AN (b) indicate the reversibility of the phase transitions. The onset temperatures are shown.

The phase transitions AX·3AN-(I)  $\rightarrow$  AX·3AN-(II) upon cooling follow the Ostwald–Volmer rule, with the thermodynamically stable phase having the higher density.

### 3.3. Crystal Structures

#### 3.3.1. AFP·AN

The monoclinic room-temperature polymorph AFP·AN-(I) comprises three  $\text{NH}_4^+$  cations, one  $\text{PO}_3\text{F}^{2-}$  anion, and one  $\text{NO}_3^-$  anion in the asymmetric unit. Corresponding bond lengths and angles are compiled in Table 3. In the monofluorophosphates anion ( $-73^\circ\text{C}$  data), the average P–O bond length (1.506 Å), the P–F bond length (1.5953(6) Å), the average O–P–O angle ( $114.7^\circ$ ), and the average O–P–F angle ( $103.5^\circ$ ) are in very good agreement with the literature values calculated for 88 independent  $\text{PO}_3\text{F}^{2-}$  anions or entities (P–O = 1.506(13) Å; P–F = 1.578(20) Å; O–P–O =  $113.7(1.7)^\circ$ ; and O–P–F =  $104.8(1.7)^\circ$ ) [6]. The same applies to the average N–O bond length (1.246 Å; literature value 1.247(29) Å calculated for 468 N–O bonds in nitrates [23]).

The crystal structure of AFP·AN-(I) is arranged in alternating (100) layers of cations and  $\text{PO}_3\text{F}^{2-}/\text{NO}_3^-$  anions (Figure 5a), whereby the  $\text{NO}_3^-$  anion is approximately oriented parallel to (001) (the angle between the mean plane through the nitrate anion and (001) is  $14.04(3)^\circ$ ). N–H $\cdots$ O hydrogen bonds between the ammonium cations and the anions, with every H atom involved in these interactions, consolidate the crystal structure (detailed numerical data of hydrogen-bonding interactions are compiled in the Supplementary Material, Table S5). Notably, hydrogen-bonding interactions are stronger between the  $\text{PO}_3\text{F}^{2-}$  anion (eight interactions with N $\cdots$ O distances  $\sim 2.8$  Å) than between the  $\text{NO}_3^-$

anion (four interactions with  $N\cdots O$  distances between 2.85 Å and 3.02 Å). As observed for the vast majority of monofluorophosphates, hydrogen bonds to the F atom as an acceptor are not developed [6].

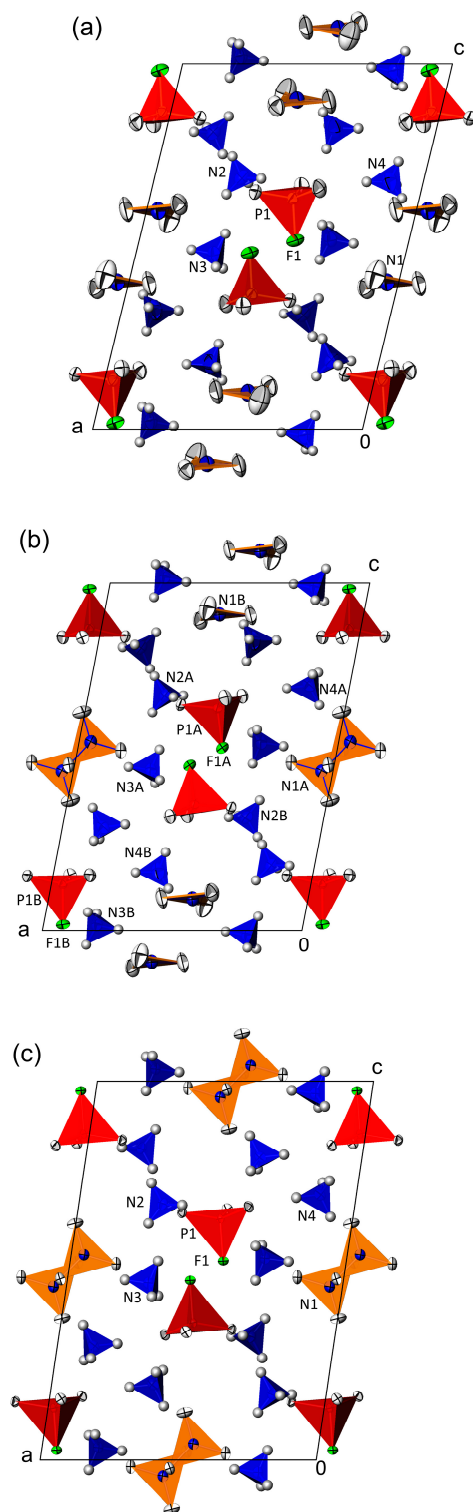


**Figure 5.** The crystal structures of AFP-AN polymorphs-(I) (a), -(II) (b), and -(III) (c) in a projection along [010]. Displacement ellipsoids are drawn at the 74% probability level. Color code:  $NH_4^+$  tetrahedra blue,  $PO_3F^{2-}$  tetrahedra red,  $NO_3^-$  triangles orange, F atoms green, and O atoms white. H atoms are given as spheres of arbitrary radius.

The phase transition from monoclinic AFP·AN-(I) to the intermediate triclinic low-temperature polymorph AFP·AN-(II) (Figure 5b) causes a doubling of the asymmetric unit, and all atomic sites in polymorph-(I) (multiplicity 4, Wyckoff letter *e*) split into two components (multiplicity 2, Wyckoff letter *i*) designated by subscripts A and B. The loss of symmetry in the crystal structure of AFP·AN-(I) in  $P2_1/n$  ( $Z = 4$ ) to AFP·AN-(II) in  $P1$  ( $Z = 4$ ) follows a group/subgroup relationship [24], with  $P1$  being a *translationengleiche* maximal subgroup of  $P2_1/n$  with index 2.

The average bond lengths, angles and BVS values for the individual molecular entities do not differ significantly from each other (Table 3) or from those of the AFP·AN-(I) polymorph ( $-98$  °C data for anions A: P–O = 1.508 Å, P–F = 1.5928(5) Å, O–P–O = 114.5°, O–P–F = 103.7°, N–O = 1.250 Å; for anions B: P–O = 1.508 Å, P–F = 1.6021(4) Å, O–P–O = 115.1°, O–P–F = 103.1°, and N–O = 1.249 Å). During the phase transition, one-half of the  $\text{NO}_3^-$  groups flipped. The general set-up of the crystal structure remains the same, but nitrate group A is now oriented nearly parallel to (010) (angle to (010) is 3.969(7)°), whereas nitrate group B remains nearly unaffected in comparison with polymorph-(I) (angle to the (001) plane is 13.42(2)°). The reorientation of nitrate group A has consequences for the hydrogen-bonding scheme (Supplementary Material, Table S6) because this group is now involved in only three but slightly stronger interactions ( $\text{N}\cdots\text{O} \sim 2.85$  Å). In turn, nitrate group B is now involved in five hydrogen-bonding interactions with slightly longer  $\text{N}\cdots\text{O}$  distances ranging from 2.85 to 3.05 Å. Again, the strongest hydrogen-bonding interactions involve the monofluorophosphates anions (eight interactions to anion A, nine to anion B), and again, N–H $\cdots$ F hydrogen bonds are not developed.

The increase in symmetry during the second phase transition from the intermediate triclinic AFP·AN-(II) to the monoclinic low-temperature AFP·AN-(III) polymorph leads to the halving of the asymmetric unit (Figure 5c) without significant changes in the average bond lengths, angles, or BVS values of the molecular moieties ( $-173$  °C data: P–O = 1.511 Å, P–F = 1.5992(5) Å, O–P–O = 114.9°, O–P–F = 103.3°, and N–O = 1.254 Å). The unique nitrate group now lies nearly parallel to (010) (deviation 4.041(8)°), and again this reorientation has consequences for the hydrogen-bonding scheme (Supplementary Material, Table S7). The nitrate group is involved in three somewhat stronger hydrogen-bonding interactions ( $\text{N}\cdots\text{O} \sim 2.82$  Å), and the  $\text{PO}_3\text{F}^{2-}$  anion shows nine hydrogen-bonding interactions, once more without the participation of the F atom.

Krivovichev introduced an approach for the comparison of the crystal structures of polymorphic compounds some years ago, making use of the topological complexity and its quantitative measures on the basis of information theory [25,26]. One of the core statements of this approach links the topological complexity of crystal structures to the “simplicity principle” introduced by Goldsmith [27]. This principle states that under conditions of rapid crystallization of polymorphic compounds, the metastable modifications form first with a simpler structure compared to the thermodynamically stable phase. The example of AFP·AN shows indeed that under the given crystallization conditions from a saturated solution, the metastable monoclinic AFP·AN-(I) polymorph forms first, which transforms exothermally into triclinic AFP·AN-(II) upon cooling. The comparison of the two crystal structures intuitively shows a higher complexity of AFP·AN-(II) due to the doubling of the contents in the asymmetric unit. In fact, this assumption can be quantitatively confirmed by complexity parameters, which all indicate a higher complexity of polymorph-(II). The corresponding numerical data were computed using the *crystIT* program [28] and are compiled in the Supplementary Material, Table S8. The subsequent phase transition AFP·AN-(II)  $\rightarrow$  AFP·AN-(III), however, cannot be correlated with the “simplicity principle” because a simpler monoclinic crystal structure is formed again upon cooling, also exothermally. Incidentally, the crystal structure of AFP·AN-(III) shows the same complexity parameters as AFP·AN-(I) (Supplementary Material, Table S8), which is a clear indication of the limitations of the “topological complexity” approach with respect to polymorphic compounds.

Polymorphs-(I) and -(III) crystallize with the same space group symmetry and with the same number of atoms at sites with the same symmetry in the asymmetric unit. Thus, their crystal structures can be quantitatively compared with the *compstru* program [20]. Numerical values for individual atomic displacements between the two crystal structures and their similarity parameters are collated in the Supplementary Material (Table S9). The  $\text{PO}_3\text{F}^{2-}$  group shows only a slight displacement (on average  $\approx 0.2$  Å). As expected from the rotation of the nitrate anion, the displacements of its atoms are by far the greatest and range from 0.89 Å for the N atom to 2.4 Å for one of the O atoms. The concomitant changes in the hydrogen-bonding schemes are indicated by shifts between 0.17 and 0.59 Å for the N atoms of the ammonium groups.

### 3.3.2. AX·3AN (X = Se, Cr)

The high-temperature forms of AX·3AN-(I) crystallize with  $Z = 2$  in space group  $P2_1$  and are isotypic with AS·3AN [7]. The asymmetric unit of this structure type comprises five  $\text{NH}_4^+$  groups, one  $\text{XO}_4^{2-}$  anion, and three  $\text{NO}_3^-$  anions. Table 4 lists corresponding bond lengths and angles. Like in the sulfate double salt, the same type of rotational disorder of one of the nitrate anions (N3) is observed, with a ratio of 0.746(6): 0.254(6) for the selenate and of 0.694(15): 0.306(15) for the chromate double salt. Since the structural features of AS·3AN have been discussed in detail [7], only the most important structural aspects are described here.

In AX·3AN-(I), the mean Se–O and Cr–O bond length in the selenate and chromate anion is 1.618 Å and 1.641 Å, respectively. These values are within the single standard deviation of the respective literature values, 1.636(23) Å calculated for 187 Se–O bonds [29], and 1.652(59) Å calculated for 169 Cr–O bonds [23].

In the crystal structure of AX·3AN-(I), cations and anions are arranged in layers extending parallel to (001) (Figure 6a). The stacking of alternating cationic and anionic layers along [001] involves a double layer of  $\text{NH}_4^+$  cations, a layer of  $\text{NO}_3^-$  and  $\text{XO}_4^{2-}$  anions, followed by two alternating  $\text{NH}_4^+$  and  $\text{NO}_3^-$  layers, an  $\text{NH}_4^+$  layer, and a layer of  $\text{NO}_3^-$  and  $\text{XO}_4^{2-}$  anions (Figure 7a). The cohesion between layers is maintained by N–H···O hydrogen bonds between ammonium cations and the complex anions (Table 4; for detailed numerical data, see Supplementary Material, Tables S10 and S12), whereby every H atom participates in the hydrogen-bonding interactions. Just like for the AFP·AN polymorphs, the hydrogen bonds involving the tetrahedral anions are somewhat stronger than those involving the nitrate anions as judged from corresponding N···O distances. A direct structural comparison of the  $P2_1$  high-temperature AX·3AN-(I) polymorphs (Supplementary Material, Table S9) reveals a higher structural similarity between the sulfate and selenate double salts ( $\delta = 0.014$ ; averaged displacement 0.073 Å) than between the sulfate and chromate double salts ( $\delta = 0.092$ ; averaged displacement 0.141 Å). Relative to the sulfate double salt, in the other two double salts, the displacements of the O atoms of the tetrahedral  $\text{XO}_4^{2-}$  group are the greatest, which we ascribe to the smaller ionic radius of 0.12 Å for  $\text{S}^{\text{VI}}$  in comparison with 0.28 Å for  $\text{Se}^{\text{VI}}$  and 0.26 Å for  $\text{Cr}^{\text{VI}}$  [30], and the concomitant shortening of the X–O bond lengths.

Upon cooling, the AX·3AN-(I) phases transform into the low-temperature forms AX·3AN-(II) (Figures 6b and 7b). The AX·3AN-(II) crystal structures are isotypic with each other and crystallize with  $Z = 4$  in the space group  $P2_1/c$ . In relation to the high-temperature AX·3AN-(I) structures, the contents of the asymmetric units are the same, but with the  $c$ -axis doubled and a shift of the unit cell of  $\sim 1/4$  along the  $b$ -axis. The arrangement of alternating cationic and anionic layers stacked along [001] in the AX·3AN-(II) crystal structure remains in the high-temperature form but with a doubled sequence in the unit cell (Figure 7). At  $-173$  °C, the mean Se–O and Cr–O bond lengths of 1.641 Å and 1.648 Å are longer than in the corresponding high-temperature polymorphs. Montejo-Bernardo et al. reported a similar behavior for the AS·3AN structure where the mean S–O distance shortens with increasing temperature. They explained this rather atypical behavior with an increase in the librational motion of the O atoms with temperature [7].

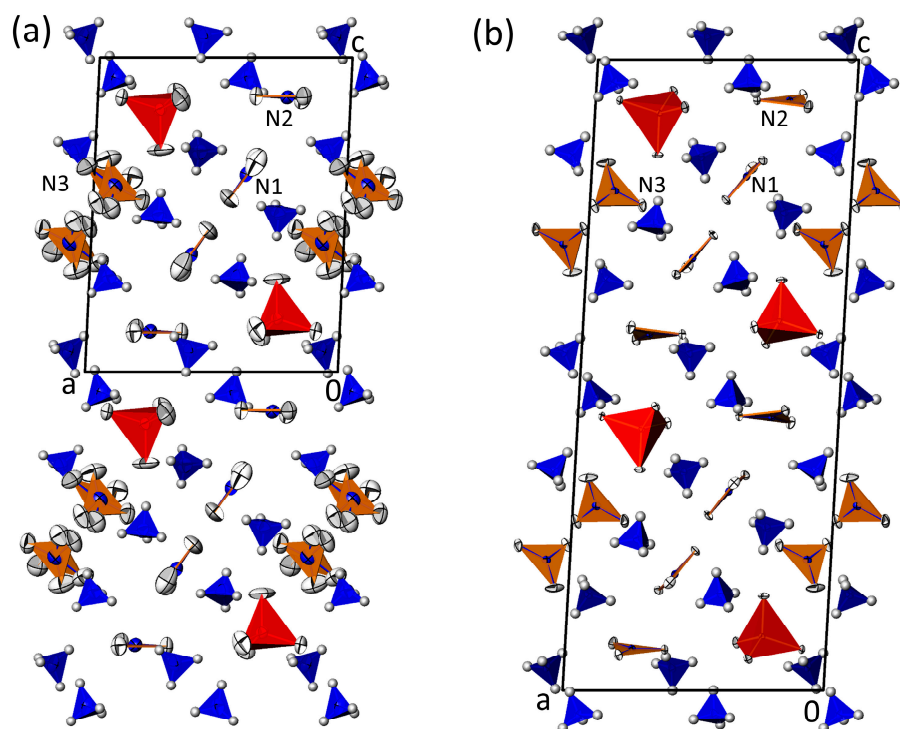


**Figure 6.** The crystal structure of the AX·3AN polymorphs-(I) (a) and -(II) (b) in a projection along [010]; data taken from the selenate double salt showing the disorder of nitrate group N3 for polymorph-(I). Displacement ellipsoids are drawn at the 74% probability level. Colour code: NH<sub>4</sub><sup>+</sup> tetrahedra blue, XO<sub>4</sub><sup>2-</sup> tetrahedra red, NO<sub>3</sub><sup>-</sup> triangles orange, F atoms green, and O atoms white. H atoms are given as spheres of arbitrary radius.

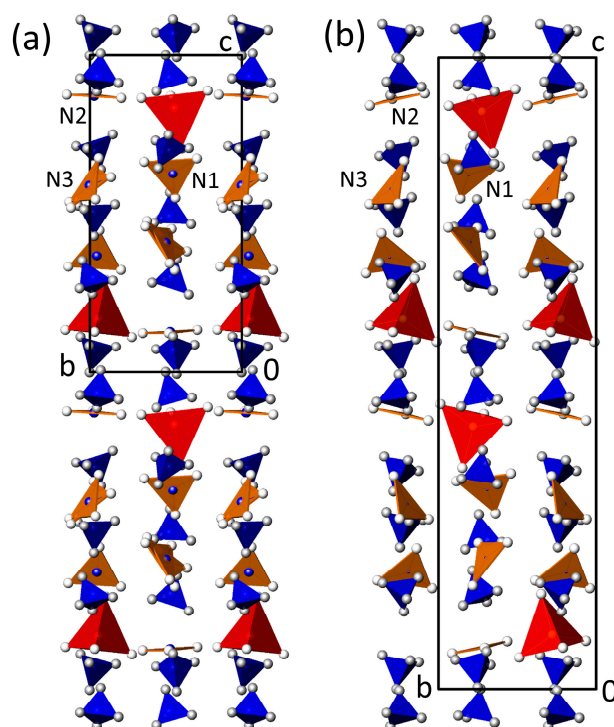


**Figure 7.** The crystal structure of the AX·3AN polymorphs-(I) (a) and -(II) (b) in a projection along [100]; data from the selenate double salt. Colour codes are the same as in Figure 6. All atoms are given as spheres of arbitrary radii.

The nitrate groups are of particular importance during the AX·3AN-(I) → AX·3AN-(II) phase transitions and subsequent cooling to  $-173\text{ }^{\circ}\text{C}$ . For the selenate double salt, at a temperature of  $-23\text{ }^{\circ}\text{C}$ , the rotational disorder of the N3 nitrate group (ratio 0.741(15):0.259(15)) remains in the doubled unit cell of AX·3AN-(II), with an additional disorder of the N1 nitrate group (ratio 0.629(15):0.371(15)). Upon further cooling to  $-73\text{ }^{\circ}\text{C}$ , both nitrate groups order, and all other molecular moieties stay ordered until  $-173\text{ }^{\circ}\text{C}$ . The situation with respect to the temperature-dependent ordering of nitrate groups is different in the chromate double salt structures. At  $-23\text{ }^{\circ}\text{C}$ , only the N1 nitrate group shows rotational disorder (ratio 0.55(3):0.45(3)) that remains nearly unchanged at all measurement temperatures down to  $-173\text{ }^{\circ}\text{C}$  (ratio 0.533(7):0.467(7)). It should be noted that a phase transition AX·3AN-(I) → AX·3AN-(II) is not reported for the sulfate double salt in the temperature range from  $23\text{ }^{\circ}\text{C}$  to  $-173\text{ }^{\circ}\text{C}$ . Nevertheless, the populations of the rotationally disordered N3 nitrate group in the  $P2_1$  structures of AS·3AN change from a ratio of 67.8:32.2 at room temperature to 82.5:17.5 at  $-173\text{ }^{\circ}\text{C}$ . Moreover, the N1 nitrate group shows disorder of one of the O atoms at room temperature, a feature that does not occur at  $-173\text{ }^{\circ}\text{C}$  [7].

The reorientation of the ordered and disordered parts of the nitrate groups in the AX·3AN polymorphs induces a slight tilt of the  $\text{XO}_4^{2-}$  anions, but also a considerable rearrangement of the ammonium cations. Since the latter define all N–H donor groups, details of the hydrogen-bonding schemes are different between the AX·3AN polymorphs, and also between the AX·3AN-(II) structures at different temperatures (Supplementary Material, Tables S11 and S13), with only slight changes in the overall N···O distances (Table 4).

Although the similarities in the crystal structures of the AX·3AN-(I) and -(II) polymorphs are apparent (Figures 6 and 7), they cannot be directly related by group/subgroup relationships [24]. Polymorph-(I) crystallizes in space group  $P2_1$  with  $Z = 2$  and polymorph-(II) in  $P2_1/c$  with  $Z = 4$ . In this relation,  $P2_1/c$  is a minimal non-isomorphic supergroup (G) of  $P2_1$  (a maximal non-isomorphic subgroup, H), so it follows that the index G:H must be  $>1$ , which is not fulfilled for the present case where the number of formula units  $Z$  for G is greater than  $Z$  for H.

Concerning the “topological complexity” approach of Krivovichev [25,26], the phase transitions AX·3AN-(I) → AX·3AN-(II) behave conformally to the “simplicity principle”. All numerical complexity parameters (Supplementary Material, Table S8) of the crystal structures of AX·3AN-(II) with their doubled monoclinic unit cells are greater than those of the structurally simpler metastable polymorphs AX·3AN-(I).

### 3.4. IR Spectroscopy of AFP·AN-(I)

The IR spectrum of AFP·AN-(I) (Figure 8) shows nine bands that can be assigned to the individual molecular moieties  $\text{NH}_4^+$ ,  $\text{NO}_3^-$ , and  $\text{PO}_3\text{F}^{2-}$ , as detailed in Table 5.

**Table 5.** AFP·AN-(I); infrared vibrational bands and their assignments.

Band	Wavenumber/ $\text{cm}^{-1}$	Assignment
1, 2, 3	3186, 3004, 2810	$\nu$ N–H
4	1450	$\delta$ H–N–H
5	1335	$\nu_{\text{as}}$ O–N–O
6	1136	$\nu_{\text{as}}$ P–O
7	1020	$\nu_{\text{s}}$ P–O
8	762	$\nu$ P–F
9	530	$\delta$ O–P–O

Bands 1–4 and 5 are characteristic of the ammonium cation and the nitrate anion, as reported for various polymorphs of  $\text{NH}_4\text{NO}_3$  [31]. The bands 6–9 are clearly assignable to the monofluorophosphate anion and are likewise in characteristic ranges for the P–O and P–F vibrations [6,32–36]. Although the P–F stretching vibration of the  $\text{PO}_3\text{F}^{2-}$  anion in solid monofluorophosphates generally tends to vary ( $\text{SrPO}_3\text{F}$ :  $844\text{ cm}^{-1}$  [32];  $\text{CdPO}_3\text{F}(\text{H}_2\text{O})_2$ :

825  $\text{cm}^{-1}$  [6];  $\text{Hg}_2\text{PO}_3\text{F}$ : 824  $\text{cm}^{-1}$  [33];  $\text{MnPO}_3\text{F}(\text{H}_2\text{O})_2$ : 802  $\text{cm}^{-1}$  [34],  $\text{Sr}(\text{PO}_3\text{F})\cdot\text{H}_2\text{O}$ : 801  $\text{cm}^{-1}$  [32];  $\text{Ag}_2\text{PO}_3\text{F}$ : 792  $\text{cm}^{-1}$  [35];  $\text{NH}_4\text{Ag}_3(\text{PO}_3\text{F})_2$ : 776  $\text{cm}^{-1}$  [36]), the one in  $\text{AFP}\cdot\text{AN}(\text{I})$  has the lowest value (762  $\text{cm}^{-1}$ ) of any monofluorophosphate reported to date. The observed red-shifted P–F vibrational band in  $\text{AFP}\cdot\text{AN}(\text{I})$  can be correlated with the comparatively long P–F bond that is about 0.02 Å longer than the overall arithmetic mean of 1.578(20) Å [6].

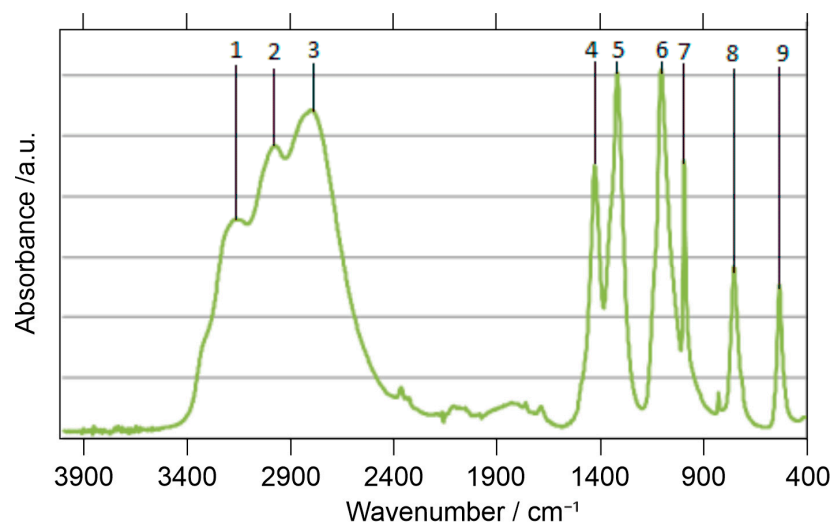


**Figure 8.** ATR infrared spectrum of  $\text{AFP}\cdot\text{AN}(\text{I})$ .

#### 4. Conclusions

For  $(\text{NH}_4)_2\text{SO}_4$  (AS)/ $\text{NH}_4\text{NO}_3$  (AN), the double salts  $(\text{NH}_4)_2\text{SO}_4\cdot 2\text{NH}_4\text{NO}_3$  (AS·2AN) and  $(\text{NH}_4)_2\text{SO}_4\cdot 3\text{NH}_4\text{NO}_3$  (AS·3AN) crystallize in aqueous solutions [7]. For the related system  $(\text{NH}_4)_2\text{PO}_3\text{F}$  (AFP)/ $\text{NH}_4\text{NO}_3$ , where the  $\text{SO}_4^{2-}$  anion is replaced with isoelectronic  $\text{PO}_3\text{F}^{2-}$ , the double salt formation occurs as well, but with a different ratio of 1:1 for  $\text{AFP}\cdot\text{AN}$ . This compound undergoes two reversible structural phase transitions upon cooling and reheating (monoclinic polymorph (I) in the space group  $P2_1/c$  ( $Z = 4$ )  $\rightleftharpoons$  triclinic polymorph (II) in the space group  $P1$  ( $Z = 4$ )  $\rightleftharpoons$  monoclinic polymorph (III) in the space group  $P2_1/c$  ( $Z = 4$ )).

If, on the other hand, the tetrahedral  $\text{SO}_4^{2-}$  anion is replaced by tetrahedral oxo anions  $\text{XO}_4^{2-}$  ( $X = \text{Se}, \text{Cr}$ ), the compounds  $(\text{NH}_4)_2\text{SeO}_4\cdot 3\text{NH}_4\text{NO}_3$  (ASe·3AN) and  $(\text{NH}_4)_2\text{CrO}_4\cdot 3\text{NH}_4\text{NO}_3$  (ACr·3AN) are obtained, establishing an isostructural relationship with AS·3AN. In the monoclinic crystal structures (space group  $P2_1$ ,  $Z = 2$ ) of the sulfate (room temperature data), selenate (40 °C data), and chromate (60 °C data) double salts, one of the nitrate groups is rotationally disordered over two positions. In contrast to AS·3AN, which shows no structural phase transition upon cooling to  $-173$  °C [7], both ASe·3AN and ACr·3AN transform into a monoclinic polymorph with a doubled unit cell (space group  $P2_1/c$ ,  $Z = 4$ ) upon cooling.

In the crystal structure of  $\text{AFP}\cdot\text{AN}$ , the hydrogen bonds of the type  $\text{N}-\text{H}\cdots\text{F}$  are not developed, in agreement with the vast majority of other monofluorophosphates where hydrogen-bonding interactions are present [6]. This almost characteristic and structure-directing behavior might be the main reason why phases “ $\text{AFP}\cdot 3\text{AN}$ ” and “ $\text{AFP}\cdot 2\text{AN}$ ” do not crystallize because in the  $\text{AX}\cdot 3\text{AN}$  structures (valid for both polymorphs) and in AS·2AN [7] all O atoms of the tetrahedral anions are involved in (comparatively strong) hydrogen-bonding interactions.

The driving force for the phase transitions in the  $\text{AFP}\cdot\text{AN}$  and  $\text{AX}\cdot 3\text{AN}$  double salts is conditioned by the nitrate groups. Whereas in  $\text{AFP}\cdot\text{AN}$ , the phase transitions (I)  $\rightleftharpoons$  (II) and (II)  $\rightleftharpoons$  (III) can be correlated with a reorientation of the  $\text{NO}_3^-$  groups within the crystal structures relative to the other building units, in the  $\text{AX}\cdot 3\text{AN}$  polymorphs the order/disorder phenomena of nitrate groups are primarily made responsible for the phase

transitions. Due to the rearrangement and order/disorder of the nitrate groups in the respective polymorphs, there is also a reorientation of the tetrahedral anions, but especially of the ammonium cations. Although this has an impact on the hydrogen-bonding network in detail, the overall N···O distances in the different polymorphs do not change drastically.

**Supplementary Materials:** The following supporting information can be downloaded at: <https://www.mdpi.com/article/10.3390/inorganics11110433/s1>, Figure S1: PXRD simulations based on single-crystal data for the different  $(\text{NH}_4)_2\text{PO}_3\text{F}\cdot\text{NH}_4\text{NO}_3$  polymorphs; Figure S2: TG curve (black) and DSC curve (blue) of  $(\text{NH}_4)_2\text{PO}_3\text{F}\cdot\text{NH}_4\text{NO}_3$ -I in the temperature range 30–550 °C; Figure S3: Evolution of the refined unit cell volume (Rietveld method) of  $(\text{NH}_4)_2\text{SeO}_4\cdot 3\text{NH}_4\text{NO}_3$  across the phase transition between 37 °C and 40 °C. Blue symbols represent polymorph-(I), red symbols polymorph-(II). For better comparison, the unit cell volume of polymorph-(II) was doubled; Table S1: Data collection and refinement details of  $(\text{NH}_4)_2\text{PO}_3\text{F}\cdot\text{NH}_4\text{NO}_3$ -I at 22 °C; Table S2: Data collection and refinement details of  $(\text{NH}_4)_2\text{SeO}_4\cdot 3\text{NH}_4\text{NO}_3$ -II at different temperatures; Table S3: Data collection and refinement details of  $(\text{NH}_4)_2\text{CrO}_4\cdot 3\text{NH}_4\text{NO}_3$ -II at different temperatures; Table S4: Selected bond lengths and interactions /Å of  $(\text{NH}_4)_2\text{PO}_3\text{F}\cdot\text{NH}_4\text{NO}_3$ -II at 22 °C and of  $(\text{NH}_4)_2\text{XO}_4\cdot 3\text{NH}_4\text{NO}_3$ -II at different temperatures; Table S5:  $(\text{NH}_4)_2\text{PO}_3\text{F}\cdot\text{NH}_4\text{NO}_3$ -I. Numerical details of hydrogen bonding interactions at 22 °C and at −73 °C; Table S6:  $(\text{NH}_4)_2\text{PO}_3\text{F}\cdot\text{NH}_4\text{NO}_3$ -II. Numerical details of hydrogen-bonding interactions at −98 °C; Table S7:  $(\text{NH}_4)_2\text{PO}_3\text{F}\cdot\text{NH}_4\text{NO}_3$ -III. Numerical details of hydrogen-bonding interactions at −173 °C; Table S8: Complexity parameters calculated with the *crystIT* program; Table S9: Absolute atomic displacements ( $|u|$  /Å) of the pair  $(\text{NH}_4)_2\text{PO}_3\text{F}\cdot\text{NH}_4\text{NO}_3$ -I and -III, and of  $(\text{NH}_4)_2\text{XO}_4\cdot 3\text{NH}_4\text{NO}_3$  crystal structures in space group  $P2_1$  (reference structure  $(\text{NH}_4)_2\text{SO}_4\cdot 3\text{NH}_4\text{NO}_3$ ), as well as their lattice distortion ( $S$ ), arithmetic mean distance  $d_{av}$  /Å and measure of similarity ( $\delta$ ). For all calculations, H atoms in the crystal structures were not considered for comparison; for the disordered nitrate group in the  $(\text{NH}_4)_2\text{XO}_4\cdot 3\text{NH}_4\text{NO}_3$  structures, only atoms of the major orientation were taken into account; Table S10:  $(\text{NH}_4)_2\text{SeO}_4\cdot 3\text{NH}_4\text{NO}_3$ -I. Numerical details of hydrogen-bonding interactions at 50 °C; Table S11:  $(\text{NH}_4)_2\text{SeO}_4\cdot 3\text{NH}_4\text{NO}_3$ -II. Numerical details of hydrogen-bonding interactions at −173 °C; Table S12:  $(\text{NH}_4)_2\text{CrO}_4\cdot 3\text{NH}_4\text{NO}_3$ -I. Numerical details of hydrogen-bonding interactions at 60 °C; Table S13:  $(\text{NH}_4)_2\text{CrO}_4\cdot 3\text{NH}_4\text{NO}_3$ -II. Numerical details of hydrogen-bonding interactions at −173 °C.

**Author Contributions:** Conceptualization, M.W.; methodology, M.W.; software, M.W. and E.F.; validation, M.W. and E.F.; formal analysis, M.W.; investigation, M.W., T.H., B.B. and E.F.; resources, M.W.; data curation, M.W. and E.F.; writing—original draft preparation, M.W. and E.F.; writing—review and editing, M.W.; visualization, M.W. and E.F.; supervision, M.W.; project administration, M.W. All authors have read and agreed to the published version of the manuscript.

**Funding:** This research received no external funding.

**Data Availability Statement:** Part of the data presented in this study are available in The Cambridge Crystallographic Data Centre (CCDC) and can be obtained free of charge via [www.ccdc.cam.ac.uk/structures](http://www.ccdc.cam.ac.uk/structures).

**Acknowledgments:** The authors acknowledge the X-ray centre of TU Wien for providing free access to the single-crystal and powder diffractometers, and Berthold Stöger for helping to perform *crystIT* calculations.

**Conflicts of Interest:** The authors declare no conflict of interest.

## References

1. Schrödter, K.; Bettermann, G.; Staffel, T.; Wahl, F.; Klein, T.; Hofmann, T. *Phosphoric Acid and Phosphates in Ullmann's Encyclopedia of Industrial Chemistry*; Wiley-VCH: Weinheim, Germany, 2008; Volume 26, pp. 698–699.
2. Xiong, L.; Chen, J.; Lu, J.; Pan, C.-Y.; Wu, L.-M. Monofluorophosphates: A New Source of Deep-Ultraviolet Nonlinear Optical Materials. *Chem. Mater.* **2018**, *30*, 7823–7830. [[CrossRef](#)]
3. Lange, W. Über die Monofluorphosphorsäure und die Ähnlichkeit ihrer Salze mit den Sulfaten. *Ber. Dtsch. Chem. Ges.* **1929**, *62B*, 793–801. [[CrossRef](#)]
4. Rây, R.C. Isomorphism and Chemical Homology. *Nature* **1930**, *126*, 310–311. [[CrossRef](#)]
5. Lima-de-Faria, J.; Hellner, E.; Liebau, F.; Makovicky, E.; Parthé, E. Nomenclature of Inorganic Structure Types—Report of the International Union of Crystallography Commission on Crystallographic Nomenclature Subcommittee on the Nomenclature of Inorganic Structure Types. *Acta Crystallogr.* **1990**, *A46*, 1–11. [[CrossRef](#)]

6. Weil, M. Monofluorophosphates—New Examples and a Survey of the  $\text{PO}_3\text{F}_2^-$  Anion. *Chemistry* **2021**, *3*, 45–73. [[CrossRef](#)]
7. Montejó-Bernardo, J.M.; García-Granda, S.; Fernández-González, A. Structures of relevant ammonium salts in fertilizers. *Acta Crystallogr.* **2010**, *B66*, 358–365. [[CrossRef](#)]
8. Schülke, U.; Kayser, R. Herstellung von Fluorophosphaten, Difluorophosphaten, Fluorophosphonaten und Fluorophosphiten in fluoridhaltigen Harnstoffschmelzen. *Z. Anorg. Allg. Chem.* **1991**, *600*, 221–226. [[CrossRef](#)]
9. Berndt, A.F.; Sylvester, J.M. The crystal structure of ammonium monofluorophosphate:  $(\text{NH}_4)_2\text{PO}_3\text{F}(\text{H}_2\text{O})$ . *Acta Crystallogr.* **1972**, *B28*, 2191–2193. [[CrossRef](#)]
10. Degen, T.; Sadki, M.; Bron, E.; König, U.; Nénert, G. The HighScore suite. *Powder Diffr.* **2014**, *29*, S13–S18. [[CrossRef](#)]
11. Bruker. APEX2, SAINT and TWINABS; Bruker AXS Inc.: Madison, WI, USA, 2014.
12. Krause, L.; Herbst-Irmer, R.; Sheldrick, G.M.; Stalke, D. Comparison of silver and molybdenum microfocus X-ray sources for single-crystal structure determination. *J. Appl. Crystallogr.* **2015**, *48*, 3–10. [[CrossRef](#)]
13. Sheldrick, G.M. A short history of SHELX. *Acta Crystallogr.* **2008**, *A64*, 112–122. [[CrossRef](#)] [[PubMed](#)]
14. Sheldrick, G.M. Crystal structure refinement with SHELXL. *Acta Crystallogr.* **2015**, *C71*, 3–8.
15. *ATOMS for Windows*; Shape Software: Kingsport, TN, USA, 2006.
16. Mighell, A.D. The Reduced Cell: Its Use in the Identification of Crystalline Materials. *J. Appl. Crystallogr.* **1976**, *9*, 491–498. [[CrossRef](#)]
17. Spek, A.L. Structure validation in chemical crystallography. *Acta Crystallogr.* **2009**, *D65*, 148–155. [[CrossRef](#)]
18. Brown, I.D. *The Chemical Bond in Inorganic Chemistry: The Bond Valence Model*; Oxford University Press: Oxford, UK, 2002.
19. Brese, N.E.; O’Keeffe, M. Bond-Valence Parameters for Solids. *Acta Crystallogr.* **1991**, *B47*, 192–197. [[CrossRef](#)]
20. de la Flor, G.; Orobengoa, D.; Tasci, E.; Perez-Mato, J.M.; Aroyo, M.I. Comparison of structures applying the tools available at the Bilbao Crystallographic Server. *J. Appl. Crystallogr.* **2016**, *49*, 653–664. [[CrossRef](#)]
21. Aroyo, M.I.; Perez-Mato, J.M.; Capillas, C.; Kroumova, E.; Ivantchev, S.; Madariaga, G.; Kirov, G.; Wondratschek, H. Bilbao Crystallographic Server I: Databases and crystallographic computing programs. *Z. Kristallogr.* **2006**, *221*, 15–27. [[CrossRef](#)]
22. Lange, W.; Livingston, R. Studies of Fluorophosphoric Acids and Their Derivatives. XIII. Preparation of Anhydrous Monofluorophosphoric Acid. *J. Am. Chem. Soc.* **1946**, *69*, 1073–1076. [[CrossRef](#)]
23. Gagné, O.C.; Hawthorne, F.C. Bond-length distributions for ions bonded to oxygen: Results for the transition metals and quantification of the factors underlying bond-length variation in inorganic solids. *IUCr* **2020**, *7*, 581–629. [[CrossRef](#)]
24. Müller, U. *Symmetry Relationships between Crystal Structures. Applications of Crystallographic Group Theory in Crystal Chemistry*; Oxford University Press: Oxford, UK, 2013.
25. Krivovichev, S.V. Topological complexity of crystal structures: Quantitative approach. *Acta Crystallogr.* **2012**, *A68*, 393–398. [[CrossRef](#)]
26. Krivovichev, S.V. Which Inorganic Structures are the Most Complex? *Angew. Chem. Int. Ed.* **2014**, *53*, 654–661. [[CrossRef](#)] [[PubMed](#)]
27. Goldsmith, J.R. A “Simplexity Principle” and Its Relation to “Ease” of Crystallization. *J. Geol.* **1953**, *61*, 439–451. [[CrossRef](#)]
28. Kaußler, C.; Kieslich, G. crystIT: Complexity and configurational entropy of crystal structures via information theory. *J. Appl. Crystallogr.* **2021**, *54*, 306–316. [[CrossRef](#)] [[PubMed](#)]
29. Gagné, O.C.; Hawthorne, F.C. Bond-length distributions for ions bonded to oxygen: Metalloids and post-transition metals. *Acta Crystallogr.* **2018**, *B74*, 63–78. [[CrossRef](#)]
30. Shannon, R.D. Revised Effective Ionic Radii and Systematic Studies of Interatomic Distances in Halides and Chalcogenides. *Acta Crystallogr.* **1976**, *A32*, 751–767. [[CrossRef](#)]
31. Théorêt, A.; Sandorfy, C. Infrared spectra and crystalline phase transitions of ammonium nitrate. *Can. J. Chem.* **1964**, *42*, 57–62. [[CrossRef](#)]
32. Jantz, S.G.; van Wüllen, L.; Fischer, A.; Libowitzky, E.; Baran, E.J.; Weil, M.; Höpfe, H.A. Syntheses, Crystal Structures, NMR Spectroscopy, and Vibrational Spectroscopy of  $\text{Sr}(\text{PO}_3\text{F})\cdot\text{H}_2\text{O}$  and  $\text{Sr}(\text{PO}_3\text{F})$ . *Eur. J. Inorg. Chem.* **2016**, *7*, 1121–1128. [[CrossRef](#)]
33. Weil, M.; Puchberger, M.; Baran, E.J. Preparation and Characterization of Dimercury(I) Monofluorophosphate(V),  $\text{Hg}_2\text{PO}_3\text{F}$ : Crystal Structure, Thermal Behavior, Vibrational Spectra, and Solid-State  $^{31}\text{P}$  and  $^{19}\text{F}$  NMR Spectra. *Inorg. Chem.* **2004**, *43*, 8330–8335. [[CrossRef](#)]
34. Weil, M.; Baran, E.J.; Kremer, R.K.; Libowitzky, E. Synthesis, Crystal Structure, and Properties of  $\text{Mn}(\text{PO}_3\text{F})(\text{H}_2\text{O})_2$ . *Z. Anorg. Allg. Chem.* **2015**, *641*, 184–191. [[CrossRef](#)]
35. Weil, M.; Puchberger, M.; Füglein, E.; Baran, E.J.; Vannahme, J.; Jakobsen, H.J.; Skibsted, J. Single-Crystal Growth and Characterization of Disilver(I) Monofluorophosphate(V),  $\text{Ag}_2\text{PO}_3\text{F}$ : Crystal Structure, Thermal Behavior, Vibrational Spectroscopy, and Solid-State  $^{19}\text{F}$ ,  $^{31}\text{P}$ , and  $^{109}\text{Ag}$  MAS NMR Spectroscopy. *Inorg. Chem.* **2007**, *46*, 801–808. [[CrossRef](#)]
36. Baran, E.J.; Weil, M. Vibrational spectra of the layered monofluorophosphate(V),  $\text{NH}_4\text{Ag}_3(\text{PO}_3\text{F})_2$ . *J. Raman Spectr.* **2009**, *40*, 1698–1700. [[CrossRef](#)]

**Disclaimer/Publisher’s Note:** The statements, opinions and data contained in all publications are solely those of the individual author(s) and contributor(s) and not of MDPI and/or the editor(s). MDPI and/or the editor(s) disclaim responsibility for any injury to people or property resulting from any ideas, methods, instructions or products referred to in the content.